Article

Metallothermic Reduction of MoO$_3$ on Combustion Synthesis of Molybdenum Silicides/MgAl$_2$O$_4$ Composites

Chun-Liang Yeh * and Min-Chia Chen

Department of Aerospace and Systems Engineering, Feng Chia University, Taichung 40724, Taiwan;
m0825504@fcu.edu.tw
* Correspondence: clyeh@fcu.edu.tw; Tel.: +886-4-2451-7250 (ext. 3963)

Abstract: Combustion synthesis involving metallothermic reduction of MoO$_3$ by dual reductants, Mg and Al, to enhance the reaction exothermicity was applied for the in situ production of Mo$_3$Si–, Mo$_5$Si$_3$– and MoSi$_2$–MgAl$_2$O$_4$ composites with a broad compositional range. Reduction of MoO$_3$ by Mg and Al is highly exothermic and produces MgO and Al$_2$O$_3$ as precursors of MgAl$_2$O$_4$. Molybdenum silicides are synthesized from the reactions of Si with both reduced and elemental Mo. Experimental evidence indicated that the reaction proceeded as self-propagating high-temperature synthesis (SHS) and the increase in silicide content weakened the exothermicity of the overall reaction, and therefore, lowered combustion front temperature and velocity. The XRD analysis indicated that Mo$_3$Si–, Mo$_5$Si$_3$– and MoSi$_2$–MgAl$_2$O$_4$ composites were well produced with only trivial amounts of secondary silicides. Based on SEM and EDS examinations, the morphology of synthesized composites exhibited dense and connecting MgAl$_2$O$_4$ crystals and micro-sized silicide particles, which were distributed over or embedded in the large MgAl$_2$O$_4$ crystals.

Keywords: molybdenum silicides; MgAl$_2$O$_4$; aluminothermic; magnesiothermic; self-propagating high-temperature synthesis

1. Introduction

Molybdenum silicides, Mo$_3$Si, Mo$_5$Si$_3$ and MoSi$_2$, are promising intermetallic materials for ultrahigh-temperature structural applications. Besides a high melting point over 2020 °C, they possess high strength, excellent oxidation resistance, corrosion resistance, creep resistance and good compatibility with ceramic reinforcements [1–8]. To improve the refractory property of transition metal silicides, magnesium aluminate spinel (MgAl$_2$O$_4$) has been one of the potential additives, because of its unique combination of properties, including a high melting point (2135 °C), relatively low density, chemical inertness, high hardness, high mechanical strength and good thermal shock resistance [9–12]. However, preparation of MgAl$_2$O$_4$ via either wet chemical methods or solid-state reactions required several complicated steps under the long processing time [9–12].

As an alternative, metallothermic reduction reactions (MRRs) of metal oxides with Mg and Al as reducing agents produce MgO and Al$_2$O$_3$ as precursors for the formation of MgAl$_2$O$_4$ and such oxidation reactions are highly exothermic [13,14]. When combining Mg/Al-based MRRs with combustion synthesis, such a fabrication route is effective in producing MgAl$_2$O$_4$-containing composites. Moreover, the highly-exothermic MRRs render reduction-based combustion synthesis fit for self-propagating high-temperature synthesis (SHS). Many merits such as high energy efficiency, short reaction time, simplicity of operation and high-purity products have been recognized for the SHS process [15–17]. According to Horvitz and Gotman [18], reduction-based combustion synthesis using 2TiO$_2$–Mg–4Al samples was performed to produce TiAl–Ti$_3$Al–MgAl$_2$O$_4$ composites. Omran et al. [19] conducted co-reduction of WO$_3$ and B$_2$O$_3$ by Mg in the presence of Al$_2$O$_3$ to fabricate the composites of MgAl$_2$O$_4$–W–W$_2$B. By means of adopting pre-added MgO, Zaki et al. [20] obtained MgAl$_2$O$_4$ composites with MoSi$_2$ and Mo$_5$Si$_3$ from co-reduction of SiO$_2$ and

MoO_3 by Al in argon at a pressure of 5 MPa. The high Ar pressure was to suppress the volatilization of MoO_3. Recently, Radishevskaya et al. [21] synthesized $MgAl_2O_4$ by the SHS method using the reactant mixtures consisting of MgO and Al_2O_3, along with Al as the fuel, $Mg(NO_3)_2 \cdot H_2O$ as the oxidizer, and NaCl as the mineralizer. Results indicated that NaCl of 1 wt.% contributed to the completion of the formation of $MgAl_2O_4$ and mechanical activation of the green mixture for 60 s facilitated the production of $MgAl_2O_4$ without oxide impurities.

By using Mg and Al simultaneously as dual reductants, this work aims at investigating the in situ production of $MgAl_2O_4$-containing molybdenum silicide (Mo_3Si, Mo_5Si_3, and $MoSi_2$) composites by the SHS process with reducing stages. That is, a solid-state combustion reaction involves the synthesis of $MgAl_2O_4$ from the metallothermic reduction of MoO_3 and the formation of molybdenum silicides from elemental interactions between Mo and Si. Three different silicide phases were produced and their influence on reaction exothermicity and combustion wave kinetics was explored. Compositional and microstructural analyses were performed on the final composites. Moreover, some products were selected for Vickers hardness and fracture toughness measurements.

2. Materials and Methods

The raw materials utilized by this study include MoO_3 (Acros Organics, 99.5%), Mg (Alfa Aesar, <45 μm, 99.8%), Al (Showa Chemical Co., <45 μm, 99.9%), Mo (Strem Chemicals, <45 μm, 99.9%), Si (Strem Chemicals, <45 μm, 99.5%), and Al_2O_3 (Alfa Aesar, 99%). According to different molybdenum silicides, three reaction systems, R(1), R(2), and R(3), are formulated for the synthesis of Mo_3Si–, Mo_5Si_3–, and $MoSi_2$–$MgAl_2O_4$ composites, respectively.

$$\frac{4}{3}MoO_3 + Mg + 2Al + \left(3x - \frac{4}{3}\right)Mo + xSi \rightarrow xMo_3Si + MgAl_2O_4 \tag{1}$$

$$\frac{4}{3}MoO_3 + Mg + 2Al + \left(5y - \frac{4}{3}\right)Mo + 3ySi \rightarrow yMo_5Si_3 + MgAl_2O_4 \tag{2}$$

$$\frac{13}{12}MoO_3 + Mg + \frac{3}{2}Al + \frac{1}{4}Al_2O_3 + \left(z - \frac{13}{12}\right)Mo + 2zSi \rightarrow zMoSi_2 + MgAl_2O_4 \tag{3}$$
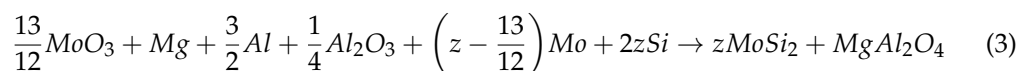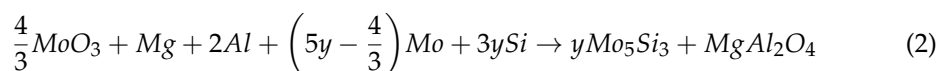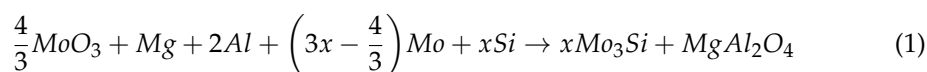
where stoichiometric coefficients x, y, and z are associated with the quantities of Mo and Si powders in the green mixtures, and also represent the molar proportion of silicide phase to $MgAl_2O_4$. The same composition of metallothermic reagents of $4/3MoO_3 + Mg + 2Al$ is adopted in R(1) and R(2), but R(3) has a different metallothermic mixture of $13/12MoO_3 + Mg + 3/2Al$ because R(3) comprises pre-added Al_2O_3. Because of metallothermic reduction of MoO_3, the source of Mo for the formation of molybdenum silicides (Mo_3Si, Mo_5Si_3, and $MoSi_2$) from R(1), R(2), and R(3) included both reduced and elemental Mo.

It has been realized that magnesiothermic and aluminothermic reductions of MoO_3 are highly exothermic and have an adiabatic temperature (T_{ad}) exceeding 4200 K [22], which plays an important role in facilitating self-sustaining combustion for R(1), R(2) and R(3). When compared with the reduction of MoO_3 by Mg and Al, the formation reactions of Mo_3Si, Mo_5Si_3 and $MoSi_2$ are much less energetic. Among three molybdenum silicides, $MoSi_2$ is the most exothermic phase to form [23], and therefore, Al_2O_3 at one-quarter of the required amount was added in the starting mixture to regulate the degree of violence of combustion.

Experimental ranges of x, y, and z conducted in this study were determined based on the reaction exothermicity of R(1), R(2) and R(3), which was assessed by computing T_{ad} as a function of stoichiometric coefficients according to the following energy balance equation [24,25] with thermochemical data taken from [23].

$$\Delta H_r + \int_{298}^{T_{ad}} \sum n_j C_p(P_j)dT + \sum\nolimits_{298-T_{ad}} n_j L(P_j) = 0 \tag{4}$$

where ΔH_r is the enthalpy of reaction at 298 K, n_j is the stoichiometric coefficient, C_p and L are the specific heat and latent heat, respectively, and P_j refers to the product.

The value of ΔH_r was calculated from the difference in enthalpy of formation (ΔH_f) between the reactants (ΔH_f of MoO_3: -745 kJ/mol, Al_2O_3: -1675.7 kJ/mol, and Mg, Al, Mo, and Si: 0 kJ/mol) and products (ΔH_f of Mo_3Si: -118.4 kJ/mol, Mo_5Si_3: -310.6 kJ/mol, $MoSi_2$: -131.4 kJ/mol, and $MgAl_2O_4$: -2299.1 kJ/mol) [23]. The values of C_p of the products as a function of temperature are expressed as follows [23].

$$C_p(Mo_3Si) = 85.23 + 22.68 \times 10^{-3} \times T + 0.03 \times 10^6 \times T^{-2} \left(J{\cdot}mol^{-1}{\cdot}K^{-1} \right) \quad (5)$$

$$C_p(Mo_5Si_3) = 183.36 + 35.01 \times 10^{-3} \times T - 1.2 \times 10^6 \times T^{-2} \left(J{\cdot}mol^{-1}{\cdot}K^{-1} \right) \quad (6)$$

$$C_p(MoSi_2) = 67.84 + 11.95 \times 10^{-3} \times T - 0.66 \times 10^6 \times T^{-2} \left(J{\cdot}mol^{-1}{\cdot}K^{-1} \right) \quad (7)$$

$$C_p(MgAl_2O_4) = 146.78 + 35.56 \times 10^{-3} \times T - 3.68 \times 10^6 \times T^{-2} \left(J{\cdot}mol^{-1}{\cdot}K^{-1} \right) \quad (8)$$

The SHS experiment was performed in a windowed combustion chamber filled with high-purity argon (99.99%) at 0.2 MPa. Reactant powders were dry mixed and then were uniaxially pressed to form cylindrical test specimens with 12 mm in height, 7 mm in diameter, and 55% in the relative density. In this work, a cylindrical bottle partially filled with the raw materials and alumina (Al_2O_3) grinding balls rotated about the longitudinal axis of a tumbler ball mill machine for 8 h to fully blend the reactant powders. The size of the alumina ball is 5 mm in diameter. The ball mill operated at 90 rpm. Because Al_2O_3 is one of the precursors to form $MgAl_2O_4$, no contamination from grinding balls was detected.

The combustion wave propagation velocity (V_f) was determined from the time series of recorded combustion videos. The combustion temperature was measured by a 125 µm bead-sized thermocouple with an alloy composition of Pt/Pt–13%Rh. Details of the experimental setup were previously reported [25,26]. Phase components of the synthesized products were identified by an X-ray diffractometer with CuK_α radiation (Bruker D2 Phaser, Billerica, MA, USA). Analyses of scanning electron microscopy (SEM) (Hitachi S3000H, Tokyo, Japan) and energy dispersive spectroscopy (EDS) were performed to examine the fracture surface microstructure and composition ratio of elements of the final products.

Measurement of Vickers hardness and fracture toughness of the products was performed [27]. For such measurements, only selected experiments under stoichiometric coefficients of $x = y = z = 2$ were carried out by placing the sample compact in a stainless-steel mold. Densification of the product was conducted by a hydraulic compressor. Upon the completion of the SHS reaction, the burned sample was rapidly pressed when the product was still hot and plastic, which was held for about 15 s. The product density after compression reached about 93–95% of theoretical density and then the product surface was polished for the measurement. Microhardness was measured with a Buehler Micromet microhardness tester at a load of 1000 g and a dwelling time of 10 s. Five indentations were made to obtain the average values of the indentation imprint and crack length measurements.

In this study, Vickers hardness (H_v) was calculated from the applied load (P) and the average diagonal impression length (d) in the equation below [28,29]. The fracture toughness (K_{IC}) was determined by the indentation method using the following equation proposed by Evans and Charles [29].

$$H_v = 1.8544 \frac{P}{d^2} \quad (9)$$

$$K_{IC} = 0.16 H_v a^{1/2} \left(\frac{c}{a} \right)^{-3/2} \quad (10)$$

where a is the half of the average length of two diagonals of the indentation and c the radial crack length measured from the center of the indentation.

3. Results and Discussion

3.1. Combustion Exothermicity of Reactions

Calculated values of T_{ad} of R(1), R(2) and R(3) as a function of their respective stoichiometric coefficients are presented in Figure 1 in order to evaluate combustion exothermicity. A significant decrease in T_{ad} with increasing silicide content is observed for all three synthesis reactions, mainly because the formation of molybdenum silicides is much less exothermic than the metallothermic reduction of MoO_3. As revealed in Figure 1, the value of T_{ad} associated with the formation of Mo_3Si–$MgAl_2O_4$ composites from R(1) decreases considerably from 3964 °C to 2415 °C as the coefficient x increases from 1 to 5. On account of a large heat capacity for Mo_5Si_3, R(2) is the weakest exothermic reaction and shows a decrease in T_{ad} from 3475 °C at $y = 1$ to 2162 °C at $y = 5$. In spite of the dilution effect of pre-added Al_2O_3 on combustion, R(3) intended for the synthesis of $MoSi_2$–$MgAl_2O_4$ composites is still very energetic with T_{ad} ranging from 3840 °C to 2745 °C. Figure 1 indicates that R(3) has the highest T_{ad} except for the case of $z = 1$. According to the analysis of combustion exothermicity, R(1) and R(3) were conducted in this study with the experimental variables of $x = 2$–5 and $z = 2$–5, respectively, and R(2) with $y = 1$–4 was carried out. Reactions with $x = 1$ and $z = 1$ were avoided, since the resulting combustion was often violent enough to melt down the powder compact and led to incomplete phase conversion.
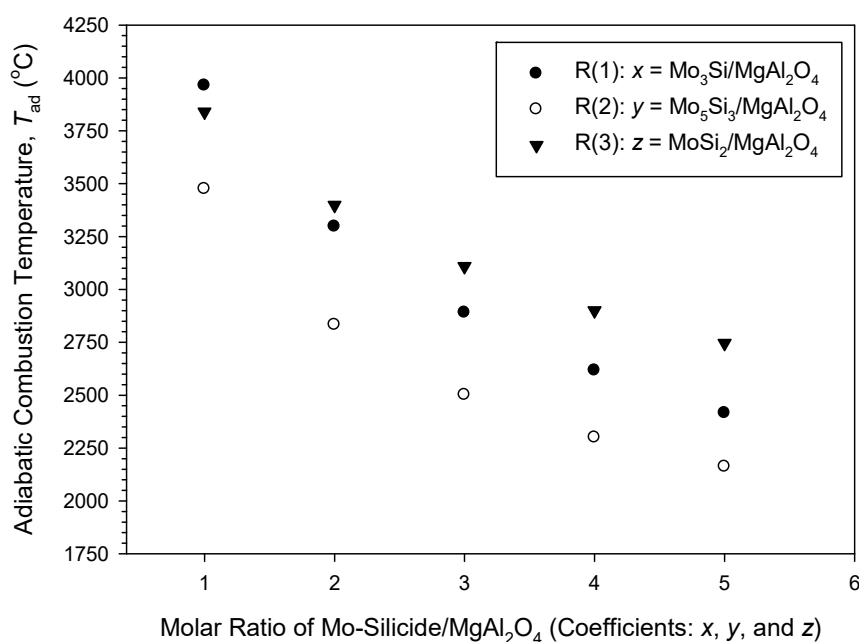
Figure 1. Variations of adiabatic combustion temperatures (T_{ad}) with molar ratios of Mo-silicide/ $MgAl_2O_4$ of products synthesized from R(1), R(2), and R(3).

3.2. Combustion Wave Velocity and Temperature

A typical sequence of recorded combustion images from R(1) with $x = 3$ is illustrated in Figure 2, showing a stable and self-sustaining combustion process. A distinct combustion front allowed the propagation velocity to be determined. Variations of combustion wave velocities of R(1), R(2) and R(3) with the molar ratio of silicide to $MgAl_2O_4$ are presented in Figure 3. A declining trend consistent with the adiabatic combustion temperature was observed. This can be explained by the fact that the combustion wave propagation rate is essentially governed by layer-by-layer heat transfer from the thin combustion zone to the unreacted region, and therefore, is subject to the reaction front temperature. Specifically, Figure 3 points out a decrease in V_f from 5.9 to 2.9 mm/s for R(1) with x from 2 to 5. For

the similar range of stoichiometry of $z = 2$–5, R(3) has a faster combustion wave with V_f ranging from 6.7 to 4.3 mm/s. On the other hand, the combustion front of R(2) has a slower speed and its V_f decreases from 5.9 mm/s at $y = 1$ to 2.7 mm/s at $y = 4$.
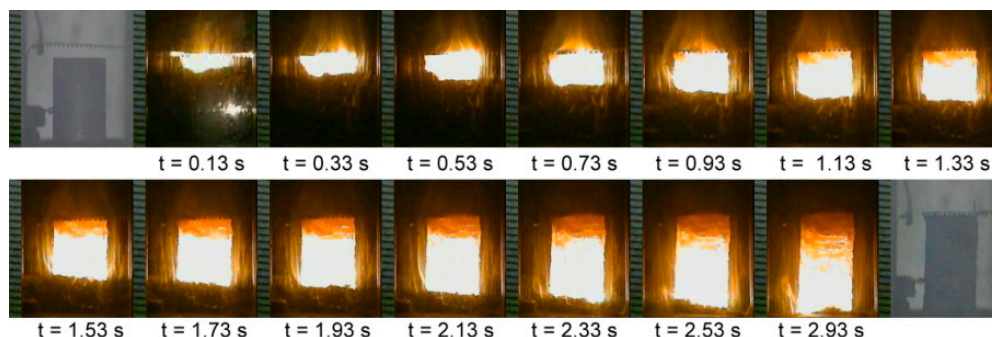
Figure 2. A typical sequence of self-sustaining combustion images recorded from R(1) with $x = 3$.
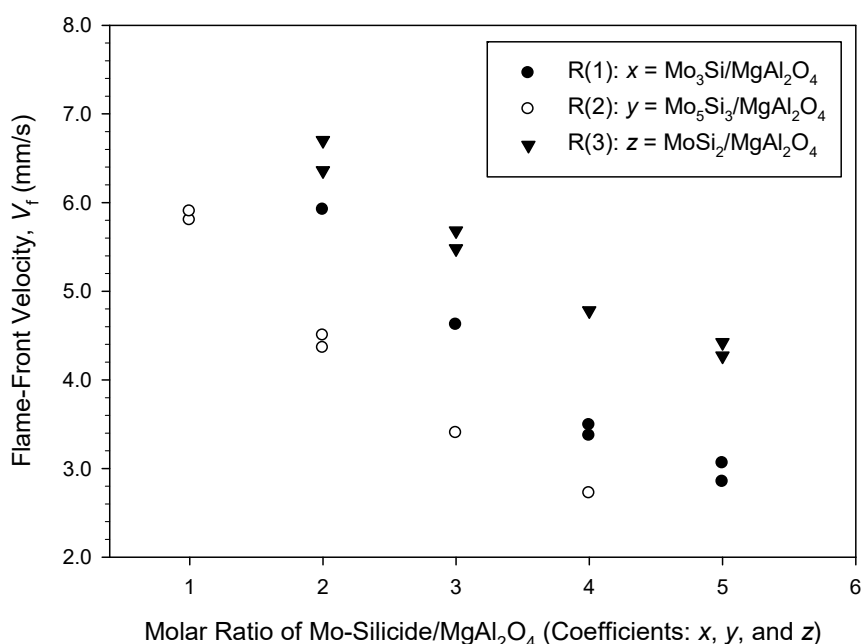
Figure 3. Variations of flame-front propagation velocities with stoichiometric coefficients (x, y, and z) of R(1), R(2), and R(3).

Figure 4a,b depict combustion temperature profiles measured from R(1), R(2) and R(3) under equal stoichiometric coefficients of 2 and 4, respectively. A steep rising gradient followed by a rapid cooling rate is characteristic of the temperature profile of the SHS reaction. The highest value is considered as the combustion front temperature (T_c). A comparison of T_c among three synthesis reactions in Figure 4a indicates that R(3) has the highest T_c of 1637 °C ($z = 2$), R(2) has the lowest 1442 °C ($y = 2$), and R(1) is in-between at 1574 °C ($x = 2$). A similar ranking of T_c can be seen in Figure 4b, which is associated with the synthesis of composites with a molar ratio silicide/$MgAl_2O_4$ equal to 4. When compared with T_c shown in Figure 4a, lower values of T_c = 1330 °C, 1103 °C and 1470 °C are observed in Figure 4b for R(1), R(2) and R(3), respectively. This confirms the decrease in reaction exothermicity with an increasing fraction of silicide formed in the composite.
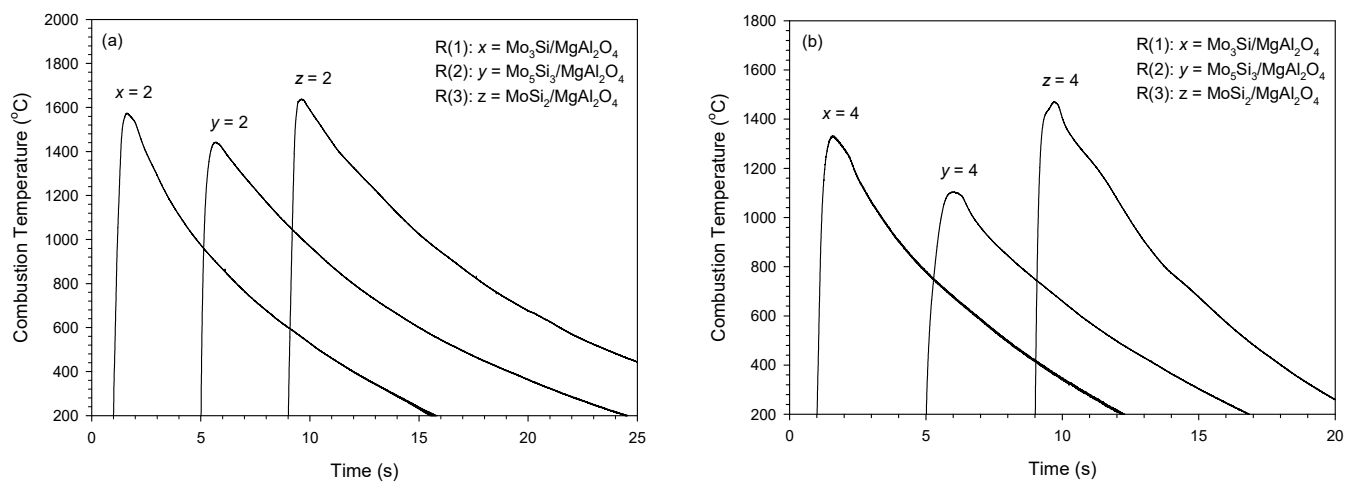
Figure 4. Combustion temperature profiles of R(1), R(2), and R(3) with stoichiometric coefficients of (**a**) $x = y = z = 2$ and (**b**) $x = y = z = 4$.

3.3. Composition and Microstructure Analyses of SHS-Derived Products

The XRD spectrum graphs of final products synthesized from R(1) with $x = 2$ and 4 are plotted in Figure 5a,b, respectively. Besides $MgAl_2O_4$, two silicide compounds were detected with Mo_3Si the dominant and Mo_5Si_3 the minor. Because of the presence of Mo_5Si_3, there was a small amount of elemental Mo left in the end product. It should be noted that the production of $MgAl_2O_4$ justifies a combination reaction between in situ formed Al_2O_3 and MgO from the metallothermic reduction of MoO_3 by dual reductants. Phase constituents associated with the products of R(2) are identified in Figure 6a,b, indicative of the Mo_5Si_3–$MgAl_2O_4$ composites with a trivial amount of Mo_3Si. Because Mo_5Si_3 has a homogeneity range from 37.5 to 40 at% Si [20], no remnant Si was found in the Mo_5Si_3–$MgAl_2O_4$ products even containing some Mo_3Si.
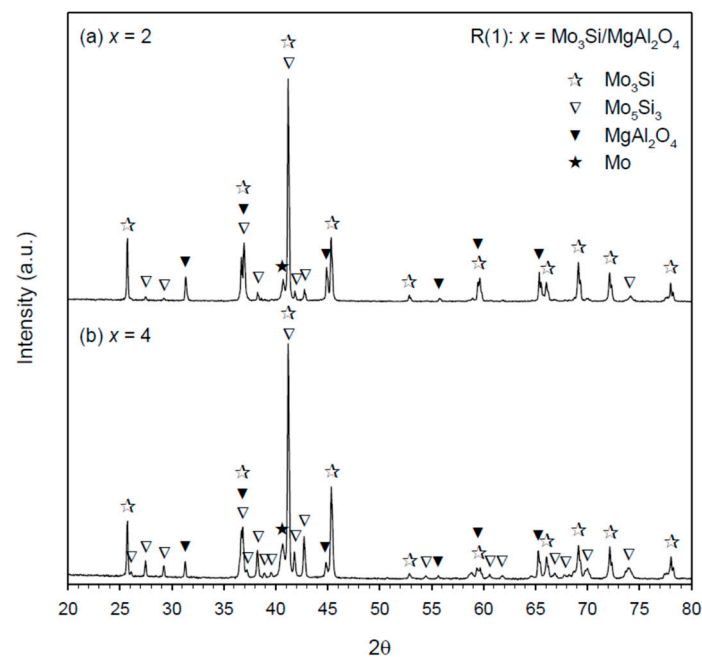
Figure 5. XRD patterns of as-synthesized Mo_3Si–$MgAl_2O_4$ composites from R(1) with (**a**) $x = 2$ and (**b**) $x = 4$.
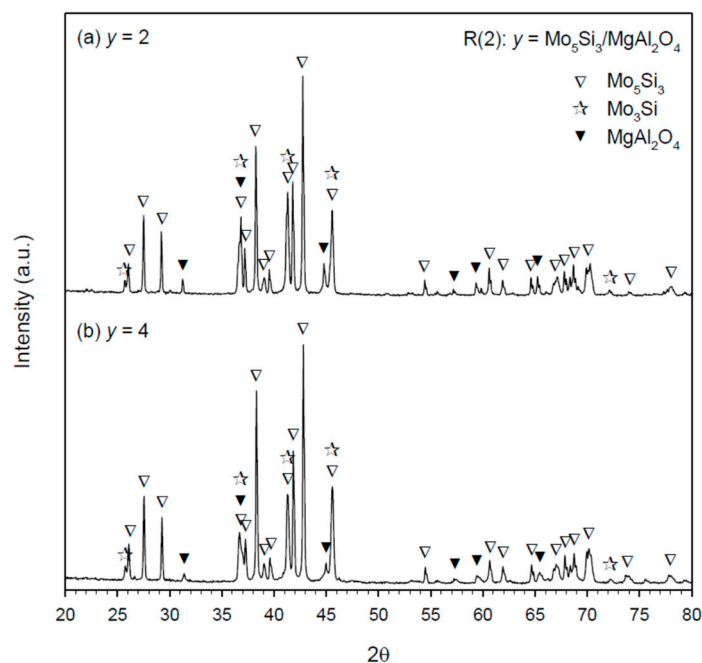
Figure 6. XRD patterns of as-synthesized Mo_5Si_3–$MgAl_2O_4$ composites from R(2) with (**a**) $y = 2$ and (**b**) $y = 4$.

Figure 7a,b shows the XRD spectra of the $MoSi_2$–$MgAl_2O_4$ composites produced from R(3) with $z = 2$ and 4, respectively. It should be pointed out that $MoSi_2$ formed from R(3) is α-$MoSi_2$ (the low-temperature phase). This was due to the fact that the reaction temperature of R(3) was below 1900 °C [22], the phase transition temperature from α-$MoSi_2$ to the high-temperature phase of β-$MoSi_2$. As revealed in Figure 7a,b, there are small amounts of Mo_5Si_3 and Si in the as-synthesized $MoSi_2$–$MgAl_2O_4$ composites.
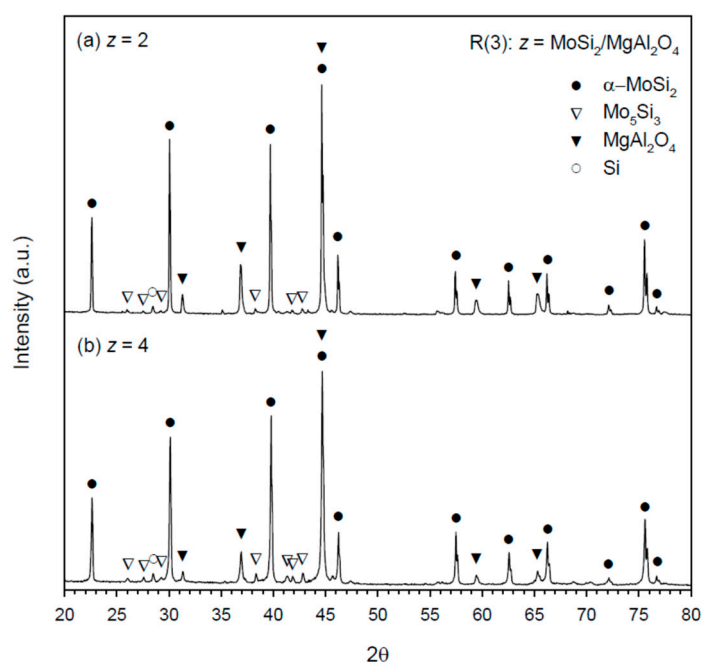
Figure 7. XRD patterns of as-synthesized $MoSi_2$–$MgAl_2O_4$ composites from R(3) with (**a**) $z = 2$ and (**b**) $z = 4$.

When compared with the work of Zaki et al. [20], $MgAl_2O_4$ composites with $MoSi_2$ and Mo_5Si_3 were produced from MoO_3, SiO_2, Al and MgO powder mixtures by self-sustaining combustion. They indicated the presence of small amounts of Mo_5Si_3, Al_2SiO_5 and free Si in the synthesized $MgAl_2O_4$–$MoSi_2$ composites. The impurity Al_2SiO_5 was formed via a combination reaction of Al_2O_3 with SiO_2. Moreover, the increase in MgO led to the formation of the other impurity Mg_2SiO_4 which was produced from the reaction between MgO and SiO_2. Therefore, it is believed that the formation of Al_2SiO_5 and Mg_2SiO_4 could be due to incomplete reduction of SiO_2, since these two phases were not found in the products of the present study. On the other hand, Zaki et al. [20] obtained $MgAl_2O_4$–Mo_5Si_3 composites without impurities and secondary silicides, on account of a larger heat release from combustion and a lesser amount of SiO_2 contained in the sample.

In the work of Radishevskaya et al. [21], MgO and Al_2O_3 were added into a combustible mixture composed of Al, $Mg(NO_3)_2 \cdot H_2O$ and NaCl to produce $MgAl_2O_4$ through the SHS scheme. Results showed that the pre-added MgO and Al_2O_3 failed to be fully combined into $MgAl_2O_4$ unless mechanical activation of initial components in a planetary mill was conducted. In contrast, MgO and Al_2O_3 were not detected in the final composites of R(1), R(2) and R(3). This could be because these two precursors of $MgAl_2O_4$ were in situ produced from metallothermic reduction reactions in the present study.

For the Mo_3Si–$MgAl_2O_4$ composite of R(1) with $x = 3$ illustrated in Figure 8, the SEM image shows the fracture surface microstructure and EDS spectra provide the atomic ratios of constitution elements. The micrograph exhibits that $MgAl_2O_4$ crystals are dense and continuous and small Mo_3Si grains tend to agglomerate into clusters. Moreover, the atomic ratios of Mo:Si = 76.16:23.84 and Mg:Al:O = 14.83:26.49:58.68 are close to those of Mo_3Si and $MgAl_2O_4$.
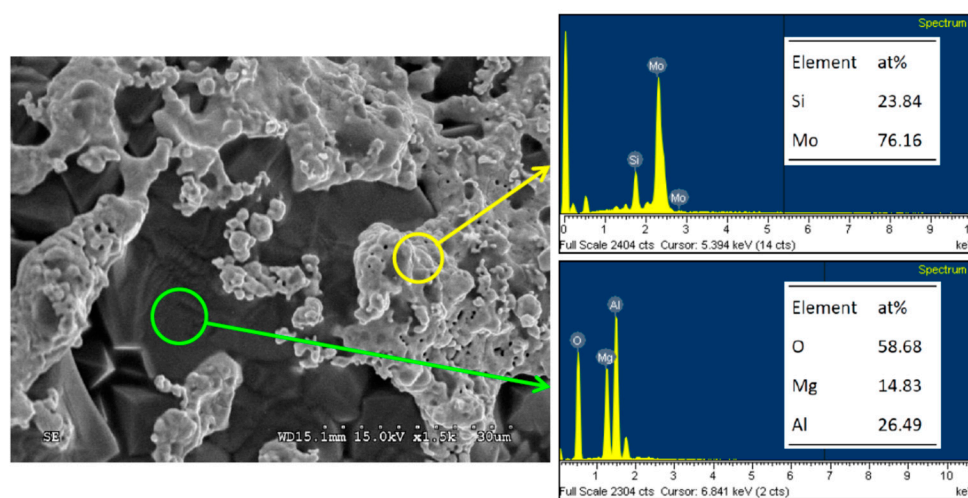
Figure 8. SEM image and EDS element spectra of Mo_3Si–$MgAl_2O_4$ composite synthesized from R(1) with $x = 3$.

The microstructure of the Mo_5Si_3–$MgAl_2O_4$ composite of R(2) with $y = 3$ in Figure 9 also reveals agglomeration of small Mo_5Si_3 grains with a particle size of about 2–4 μm. Most of the large $MgAl_2O_4$ crystals are covered with Mo_5Si_3 grains. The atomic ratios of Mo:Si = 61.64:38.36 and Mg:Al:O = 13.61:28.36:58.03 confirm the formation of Mo_5Si_3 and $MgAl_2O_4$. A similar morphology can be seen in Figure 10, unveiling the $MoSi_2$–$MgAl_2O_4$ composite of R(3) with $z = 3$. It is evident that $MgAl_2O_4$ crystals are dense and relatively large. Small $MoSi_2$ grains are distributed over or embedded in $MgAl_2O_4$ crystals. Atomic ratios of Mo:Si = 32.98:67.02 and Mg:Al:O = 13.85:28.86:57.29 were obtained from the EDS analysis.
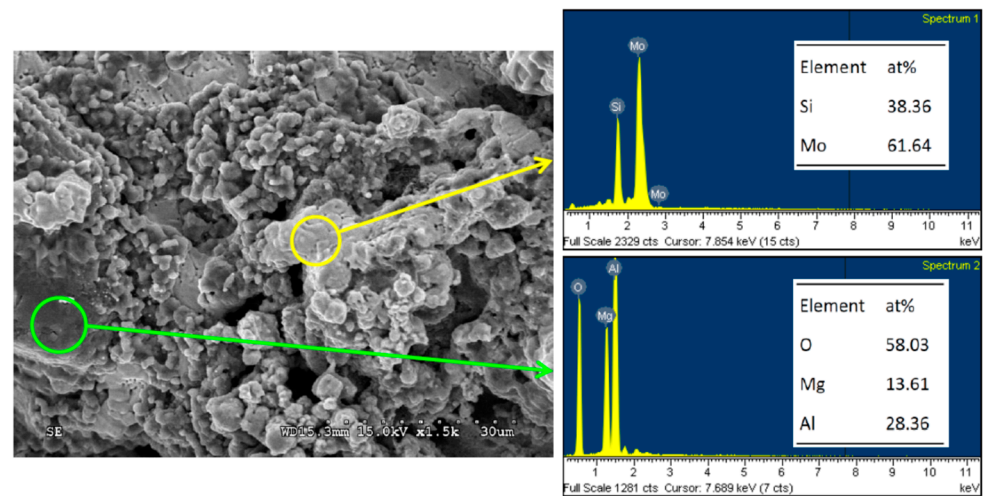
Figure 9. SEM image with EDS element spectra of Mo_5Si_3–$MgAl_2O_4$ composite synthesized from R(2) with $y = 3$.
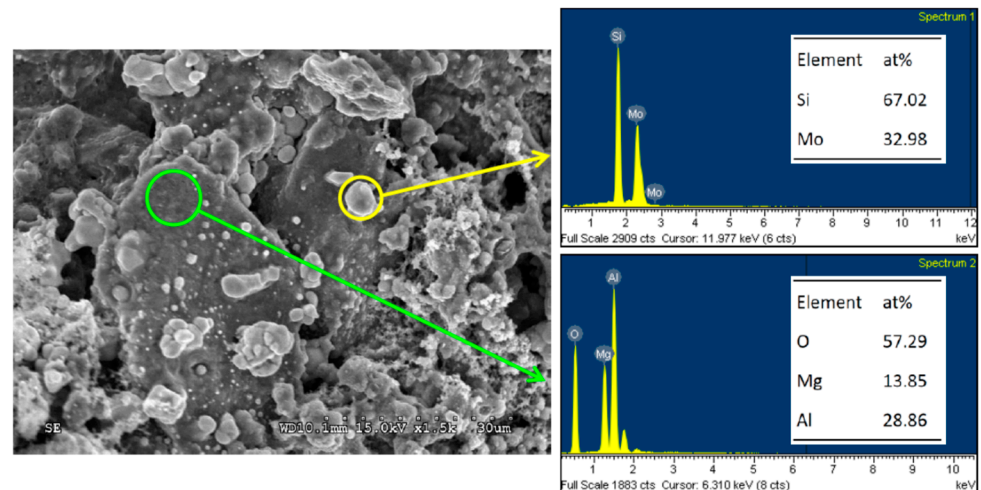
Figure 10. SEM image with EDS element spectra of $MoSi_2$–$MgAl_2O_4$ composite synthesized from R(3) with $z = 3$.

Selected test conditions ($x = y = z = 2$) were conducted to prepare product samples for the measurement of hardness and fracture toughness. For the composite of $2Mo_3Si$–$MgAl_2O_4$ produced from R(1), Vickers hardness of $H_v = 1.41 \times 10^4$ MPa and fracture toughness of $K_{IC} = 3.3$ MPa m$^{1/2}$ were determined. Values of $H_v = 1.42 \times 10^4$ MPa and $K_{IC} = 3.1$ MPa m$^{1/2}$ were obtained for $2Mo_5Si_3$–$MgAl_2O_4$ synthesized from R(2). For the product of $2MoSi_2$–$MgAl_2O_4$ from R(3), $H_v = 1.48 \times 10^4$ MPa and $K_{IC} = 2.8$ MPa m$^{1/2}$ were determined. The error of hardness values was estimated as about $\pm 10\%$ and the error of fracture toughness values was within $\pm 20\%$. The uncertainty of K_{IC} determination using the indentation fracture method could result from the residual stresses induced by specimen densification, the existence of pores or cracks, surface finish, and possible inhomogeneous microstructure. Compared with monolithic Mo_3Si, Mo_5Si_3, and $MoSi_2$ ($H_v \approx 1.3 \times 10^4$ MPa and $K_{IC} = 2\sim3$ MPa m$^{1/2}$) [7,30,31], $MgAl_2O_4$ as an additive improved the hardness and toughness of molybdenum silicides.

4. Conclusions

The in situ fabrication of Mo_3Si–, Mo_5Si_3– and $MoSi_2$–$MgAl_2O_4$ composites was investigated by the SHS process integrating metallothermic reduction of MoO_3 with combustion synthesis. Mg and Al were simultaneously used as dual reductants to produce MgO

and Al_2O_3 as precursors of $MgAl_2O_4$. Molybdenum silicides were synthesized from the elemental reactions between Mo and Si. Experimental results showed that the formation of $MoSi_2$–$MgAl_2O_4$ composites was the most exothermic and characterized by the highest combustion front temperature and fastest combustion velocity, while that of Mo_5Si_3–$MgAl_2O_4$ composites was the least. Composites with molar ratios of $Mo_3Si/MgAl_2O_4$ from 2 to 5, $Mo_5Si_3/MgAl_2O_4$ from 1 to 4, and $MoSi_2/MgAl_2O_4$ from 2 to 5 were synthesized. An increase in silicide content brought about a decrease in reaction exothermicity because the formation of molybdenum silicides was much less exothermic than the metallothermic reduction of MoO_3. Based on the XRD patterns, phase conversion from the reactants to products was essentially completed except for trivial amounts of secondary silicide and Mo or Si present in the end products. SEM and EDS analyses revealed that $MgAl_2O_4$ formed large connecting grains with a dense morphology. Granular Mo_3Si, Mo_5Si_3 and $MoSi_2$ were relatively small and were distributed over or embedded in $MgAl_2O_4$ crystals. Hardness and fracture toughness of molybdenum silicides were improved by adding $MgAl_2O_4$. This study demonstrated an effective fabrication route adopting dual reductants to increase combustion exothermicity for the in situ production of Mo_3Si–, Mo_5Si_3– and $MoSi_2$–$MgAl_2O_4$ composites with a broad compositional range.

Author Contributions: Conceptualization, C.-L.Y.; methodology, C.-L.Y. and M.-C.C.; validation, C.-L.Y. and M.-C.C.; formal analysis, C.-L.Y. and M.-C.C.; investigation, C.-L.Y. and M.-C.C.; resources, C.-L.Y.; data curation, C.-L.Y. and M.-C.C.; writing–original draft preparation, C.-L.Y. and M.-C.C.; writing–review and editing, C.-L.Y.; supervision, C.-L.Y.; project administration, C.-L.Y.; funding acquisition, C.-L.Y. Both authors have read and agreed to the published version of the manuscript.

Institutional Review Board Statement: Not applicable.

Informed Consent Statement: Not applicable.

Data Availability Statement: Data presented in this study are available in the article.

Conflicts of Interest: The authors declare no conflict of interest.

References

1. Zhang, L.; Tong, Z.; He, R.; Xie, C.; Bai, X.; Yang, Y.; Fang, D. Key issues of MoSi$_2$-UHTC ceramics for ultra high temperature heating element applications: Mechanical, electrical, oxidation and thermal shock behaviors. *J. Alloys Compd.* **2019**, *780*, 156–163. [CrossRef]
2. Tong, Z.; He, R.; Cheng, T.; Zhang, K.; Dai, D.; Yang, Y.; Fang, D. High temperature oxidation behavior of ZrB$_2$–SiC added MoSi$_2$ ceramics. *Ceram. Int.* **2018**, *44*, 21076–21082. [CrossRef]
3. Wang, L.; Fu, Q.; Zhao, F. Improving oxidation resistance of MoSi$_2$ coating by reinforced with Al$_2$O$_3$ whiskers. *Intermetallics* **2018**, *94*, 106–113. [CrossRef]
4. Liu, C.; Li, M.; Shen, Q.; Chen, H. Preparation and tribological properties of modified MoS$_2$/SiC/Epoxy composites. *Materials* **2021**, *14*, 1731. [CrossRef]
5. Zhuo, G.; Su, L.; Jiang, K.; Yang, J. Effect of spraying power on oxidation resistance of MoSi$_2$-ZrB$_2$ coating for Nb-Si based alloy prepared by atmospheric plasma. *Materials* **2020**, *13*, 5060. [CrossRef]
6. Pan, Y.; Wang, P.; Zhang, C.M. Structure, mechanical, electronic and thermodynamic properties of Mo$_5$Si$_3$ from first-principles calculations. *Ceram. Int.* **2018**, *44*, 12357–12362. [CrossRef]
7. Chen, H.; Ma, Q.; Shao, X.; Ma, J.; Wang, C.; Huang, B. Microstructure, mechanical properties and oxidation resistance of Mo$_5$Si$_3$–Al$_2$O$_3$ composites. *Mater. Sci. Eng. A* **2014**, *592*, 12–18. [CrossRef]
8. Abbasi, A.R.; Shamanian, M. Synthesis of α-Mo–Mo$_5$SiB$_2$–Mo$_3$Si nanocomposite powders by two-step mechanical alloying and subsequent heat treatment. *J. Alloys Compd.* **2011**, *509*, 8097–8104. [CrossRef]
9. Ganesh, I. A review on magnesium aluminate (MgAl$_2$O$_4$) spinel: Synthesis, processing and applications. *Int. Mater. Rev.* **2013**, *58*, 63–112. [CrossRef]
10. Mouyane, M.; Jaber, B.; Bendjemil, B.; Bernard, J.; Houivet, D.; Noudem, J.G. Sintering behavior of magnesium aluminate spinel MgAl$_2$O$_4$ synthesized by different methods. *Int. J. Appl. Ceram. Technol.* **2019**, *16*, 1138–1149. [CrossRef]
11. Padmaraj, O.; Venkateswarlu, M.; Satyanarayana, N. Structural, electrical and dielectric properties of spinel type MgAl$_2$O$_4$ nanocrystalline ceramic particles synthesized by the gel-combustion method. *Ceram. Int.* **2015**, *41*, 3178–3185. [CrossRef]

12. Jiao, Y.; Zhu, J.; Li, X.; Shi, C.; Lu, B.; Wang, F.; Abdul, W. Mechanical Properties of Al Matrix Composite Enhanced by In Situ Formed SiC, $MgAl_2O_4$, and MgO via Casting Process. *Materials* **2021**, *14*, 1767. [CrossRef] [PubMed]

13. Skrzypczyńska, K.; Świątkowski, A.; Diduszko, R.; Dąbek, L. Studies on carbon materials produced from salts with anions containing carbon atoms for carbon paste electrode. *Materials* **2021**, *14*, 2480. [CrossRef]

14. Kudyba, A.; Akhtar, S.; Johansen, I.; Safarian, J. Aluminothermic reduction of manganese oxide from selected MnO-containing slags. *Materials* **2021**, *14*, 356. [CrossRef]

15. Merzhanov, A.G. Combustion processes that synthesize materials. *J. Mater. Process. Technol.* **1996**, *56*, 222–241. [CrossRef]

16. Levashov, E.A.; Mukasyan, A.S.; Rogachev, A.S.; Shtansky, D.V. Self-propagating high-temperature synthesis of advanced materials and coatings. *Int. Mater. Rev.* **2017**, *62*, 203–239. [CrossRef]

17. Borovinskaya, I.; Gromov, A.; Levashov, E.; Maksimov, Y.; Mukasyan, A.; Rogachev, A. *Concise Encyclopedia of Self-Propagating High-Temperature Synthesis History, Theory, Technology, and Products*, 1st ed.; Elsevier: Amsterdam, The Netherlands, 2017.

18. Horvitz, D.; Gotman, I. Pressure-assisted SHS synthesis of $MgAl_2O_4$–TiAl in situ composites with interpenetrating networks. *Acta. Mater.* **2002**, *50*, 1961–1971. [CrossRef]

19. Omran, J.G.; Afarani, M.S.; Sharifitabar, M. Fast synthesis of $MgAl_2O_4$–W and $MgAl_2O_4$–W–W_2B composite powders by self-propagating high-temperature synthesis reactions. *Ceram. Int.* **2018**, *44*, 6508–6513. [CrossRef]

20. Zaki, Z.I.; Mostafa, N.Y.; Rashad, M.M. High pressure synthesis of magnesium aluminate composites with $MoSi_2$ and Mo_5Si_3 in a self-sustaining manner. *Ceram. Int.* **2012**, *38*, 5231–5237. [CrossRef]

21. Radishevskaya, N.I.; Nazarova, A.Y.; Lvov, O.V.; Kasatsky, N.G.; Kitler, V.D. Synthesis of magnesium aluminate spinel in the $MgO-Al_2O_3$-Al system using the SHS method. *J. Phys. Conf. Ser.* **2019**, *1214*, 012019. [CrossRef]

22. Wang, L.L.; Munir, Z.A.; Maximov, Y.M. Thermite reactions: Their utilization in the synthesis and processing of materials. *J. Mater. Sci.* **1993**, *28*, 3693–3708. [CrossRef]

23. Binnewies, M.; Milke, E. *Thermochemical Data of Elements and Compounds*; Wiley-VCH Verlag GmbH: Weinheim, Germany, 2002.

24. Liang, Y.H.; Wang, H.Y.; Yang, Y.F.; Zhao, R.Y.; Jiang, Q.C. Effect of Cu content on the reaction behaviors of self-propagating high-temperature synthesis in Cu-Ti-B_4C system. *J. Alloys Compd.* **2008**, *462*, 113–118. [CrossRef]

25. Yeh, C.-L.; Chen, K.-T. Synthesis of FeSi-Al_2O_3 Composites by Autowave Combustion with Metallothermic Reduction. *Metals* **2021**, *11*, 258. [CrossRef]

26. Yeh, C.L.; Lin, J.Z. Combustion synthesis of Cr-Al and Cr-Si intermetallics with Al_2O_3 additions from Cr_2O_3-Al and Cr_2O_3-Al-Si reaction systems. *Intermetallics* **2013**, *33*, 126–133. [CrossRef]

27. Yeh, C.L.; Ke, C.Y. Intermetallic/ceramic composites synthesized from Al–Ni–Ti combustion with B_4C addition. *Metals* **2020**, *10*, 873. [CrossRef]

28. Anstis, G.R.; Chantikul, P.; Lawn, B.R.; Marshall, D.B. A critical evaluation of indentation techniques for measuring fracture toughness: I, direct crack measurements. *J. Am. Ceram. Soc.* **1981**, *64*, 533–538. [CrossRef]

29. Evans, A.G.; Charles, E.A. Fracture toughness determinations by indentation. *J. Am. Ceram. Soc.* **1976**, *59*, 371–372. [CrossRef]

30. Rosales, I.; Schneibel, J.H. Stoichiometry and mechanical properties of Mo_3Si. *Intermetallics* **2000**, *8*, 885–889. [CrossRef]

31. Morris, D.G.; Leboeuf, M.; Morris, M.A. Hardness and toughness of $MoSi_2$ and $MoSi_2$–SiC composite prepared by reactive sintering of powders. *Mater. Sci Eng. A* **1998**, *251*, 262–268. [CrossRef]